

Forward-to-backward asymmetry of the (γ, n) reaction in the energy range 20–30 MeV

T. Murakami, I. Halpern, and D. W. Storm

Nuclear Physics Laboratory, University of Washington, Seattle, Washington 98195

P. T. Debevec and L. J. Morford

Nuclear Physics Laboratory, University of Illinois at Urbana-Champaign, Urbana, Illinois 61801

S. A. Wender

Los Alamos National Laboratory, Los Alamos, New Mexico 87545

D. H. Dowell

Brookhaven National Laboratory, Upton, New York 11973

(Received 14 August 1986)

The forward-to-backward asymmetry of neutrons emitted in the (γ, n) reactions on ^{nat}Pb and ^{nat}Cd targets was measured for photons in the range of 20–30 MeV, where the isovector quadrupole giant resonance is expected to lie. The asymmetry was observed to increase from small values (≈ 0.2) to large ones (≈ 0.6 and 0.8) for ^{nat}Cd and ^{nat}Pb , respectively. This phenomenon is interpreted as the interference between $E1$ and $E2$ amplitudes. From an analysis of the asymmetry the excitation energies of the $E2$ isovector resonances were estimated to be 23.5 ± 1.5 MeV and 26.5 ± 1.5 MeV for the Pb and Cd nuclei, respectively. The $E2$ isovector resonances are found to be considerably wider than the $E1$ resonances.

I. INTRODUCTION

Compared with our knowledge of the isovector dipole resonance (IVD), i.e., the well known $E1$ giant resonance, our knowledge of the isovector $E2$ resonance (IVQ) is very limited. Most of the information about the IVQ has been obtained from inelastic electron scattering.¹ The shapes of (e, e') inelastic spectra and their dependence on scattering angle show evidence for a concentration of $E2$ strength at approximately $130A^{-1/3}$ MeV for heavier nuclei.² For light nuclei the location tends to be somewhat lower. Upon dissecting these spectra into component multipoles, the authors concluded that the width of the IVQ resonance increases from ≈ 5 to ≈ 10 MeV as the nuclear mass decreases and that the $E2$ strength concentration corresponds to 70–100% of the $T=1$, $E2$ energy-weighted sum rule (EWSR) using the Goldhaber-Teller model.² Because of the uncertain backgrounds and the strengths due to other multipoles in the (e, e') spectra, it is important to study the IVQ and its parameters using an independent method.

Evidence for the IVQ resonance has also been sought using the (p, p') reaction,³ the (π^\pm, π^0) reaction,⁴ the (γ, γ) reaction,⁵ and the (p, γ) reaction.⁶ None of these has managed to provide very definite information. In inelastic proton scattering, the dominance of the isoscalar term of the nuclear force obscures the excitation of the isovector giant resonance even at high incident energies.³ No evidence for IVQ strength was uncovered in a recent study of the (π^-, π^0) reaction on ^{40}Ca , ^{60}Ni , and ^{90}Zr targets, although this reaction clearly excited the isovector monopole and dipole resonances.⁴ According to a recent (γ, γ) reaction measurement no compact $E2$ strength is

observed in calcium between 19 and 51 MeV, nor in carbon between 25 and 45 MeV.⁵ The sensitivities of the (π^-, π^0) and the (γ, γ) reactions to the strength of the IVQ are, however, so small that a substantial fraction of the IVQ sum rule would have to be concentrated within a narrow energy interval for the IVQ to be seen.^{4,5}

Angular asymmetry studies using the (p, γ) and (n, γ) reactions have the advantage over other reactions that the asymmetry depends on the amplitude of the $E2$ resonance (including its phase) rather than just on the intensity. It is difficult to peel apart resonances on the basis of observed intensities whenever the resonances are wide. Because the phase of an amplitude changes most rapidly at resonance, it can provide valuable information to help pin down the resonance location and its other parameters. When the (p, γ) reaction was used to study the IVQ, a large background coming from direct $E2$ capture made identification of resonant $E2$ capture difficult.⁶ On the other hand, as has been pointed out earlier,⁷ there is essentially no direct $E2$ amplitude in the (γ, n) and (n, γ) reactions, since the effective charge of a neutron undergoing a direct $E2$ transition in a large nucleus is negligible. Thus, the (γ, n) and (n, γ) reactions are virtually background-free when used to locate the IVQ through interference with the tail of the IVD.

Recently, Drake *et al.* have found striking evidence for the existence and location of the IVQ in ^{208}Pb , namely a sharp rise at about 23 MeV in the (n, γ_0) forward-to-backward asymmetry.⁸ Subsequently, Bergqvist *et al.* have studied the IVQ in ^{40}Ca using the same technique.⁹ The use of the (n, γ) reaction for targets lighter than Pb is difficult because the available fluxes of higher energy monoenergetic neutrons are small. We therefore decided

to use the inverse (γ, n) reaction. In this paper we report the initial results of a survey of photoneutron asymmetries at energies appropriate to the IVQ. In the next section we present the experimental details of the measurements, and in Sec. III we summarize the experimental results. A discussion of these results in terms of both a simple schematic model and the direct-semidirect (DSD) model appears in Sec. IV.

II. EXPERIMENTAL PROCEDURE AND DATA REDUCTION

The experiment was performed using the continuous electron beam from the University of Illinois MUSL-2 electron microtron and its tagged photon facility. A 39.4 MeV electron beam was focused onto a 1 cm² aluminum converter foil 0.13 mm thick to produce bremsstrahlung. To determine the energies of the photons produced, the post-bremsstrahlung electrons were momentum-analyzed and detected in the focal plane of the analyzing magnet by an array of 32 plastic scintillators. The tagged bremsstrahlung photons, after passing through a brass collimator, struck the photonuclear target located about 1.8 m downstream from the converter. Fast neutrons ejected from this target were detected by an NE-213 liquid scintillator, 30 cm in diameter and 5.1 cm thick. This scintillator was viewed by three photomultiplier tubes 12.7 cm in diameter. It was surrounded by borated paraffin and lead shielding to reduce the number of events coming from room background. To suppress the large photon yield from the targets, 5 cm of lead was placed just in front of the neutron detector. Neutron events were distinguished from photon events by pulse-shape discrimination. The neutron energies were determined by measuring the time interval between the signals from the electron counters and the neutron detector. The time resolution of the system was estimated to be about 2 ns. The usable current of the primary electron beam was limited to a few nA by the counting rate in the post-bremsstrahlung electron counters. The allowable rate was typically $\approx 2 \times 10^5$ s⁻¹ counter⁻¹. In order to maintain a sufficiently high counting rate for true events, it was necessary to use a short flight path (1.5 m) to the neutron detector. Consequently, the neutron energy resolution was poor (1.6 MeV at $E_n = 13$ MeV and 3.6 MeV at $E_n = 23$ MeV). This resolution was not sufficient to distinguish neutron yields to different final states in the residual nucleus.

The main photonuclear targets and their thicknesses were 11.1 ± 0.2 g/cm² natural lead and 32.8 ± 0.4 g/cm² natural cadmium. To investigate a possible isotopic dependence of the reaction, a 5.4 ± 0.1 g/cm² enriched (88%) ²⁰⁶Pb target was also used. The target areas were about 15×15 cm², large enough to intercept the whole photon beam since the beam spot size was estimated to be less than 7 cm in diameter.

The cross sections of the (γ, n) reaction on these targets were measured for photon energies between 20 and 30 MeV at 55° and 125°. From these cross sections the front-to-back asymmetry, defined as

$$\alpha = [Y(55^\circ) - Y(125^\circ)] / [Y(55^\circ) + Y(125^\circ)],$$

was determined. The cross section at 90° was also mea-

sured for the natural lead target in the photon energy range between 20 and 26 MeV. The attenuation of the incident photons in the target and of the photoneutrons in the target and in the lead blocks just in front of the neutron detector were evaluated using the known photon absorption cross sections¹⁰ and the total cross sections of neutrons predicted by a global optical potential.¹¹ Although the total attenuation was large (80–92%), the differences in attenuation at 55° and 125° were, in general, quite small. For example, for the natural lead runs this difference was calculated to be less than 4.5%, with the 125° target having the smaller overall attenuation.

Tagging efficiencies were measured periodically by placing a 25×30 cm² NaI detector directly in the photon beam and counting the number of photons in coincidence with the post-bremsstrahlung electrons. In order to make this measurement, it was necessary to reduce the intensity of the electron beam by about 4 orders of magnitude. Since the tagging efficiencies were quite sensitive to the position of the electron beam spot on the aluminum converter, the beam position was monitored by a pair of profile monitors every half-hour, and sidewise beam displacement was kept to less than ± 1 mm. This procedure ensured that any variations of the tagging efficiencies during a single measurement were less than 2%.

The pulse-height calibration for the neutron detector was obtained from the Compton edges of monenergetic γ rays. These appear at 0.5 MeV (¹³⁷Cs), 1.06 MeV (²²Na), and 4.20 MeV (¹²C*). The threshold for the neutron detector was set at 3.0 MeV (equivalent electron energy) to avoid a high accidental counting rate from low energy neutrons produced in the target by the great number of untagged photons. This threshold roughly corresponds to 6.5 MeV in terms of neutron energy. The counting rate for the remaining accidental coincidence events was estimated from the number of the kinematically forbidden events in the time-of-flight spectra and was corrected for. A typical time-of-flight spectrum is shown in Fig. 1.

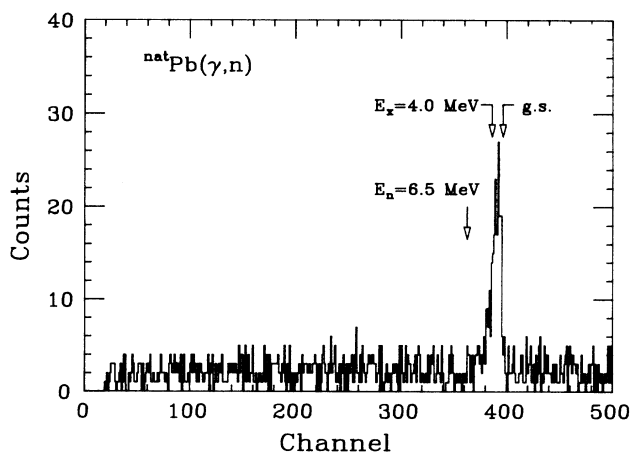


FIG. 1. A typical time-of-flight spectrum for $^{nat}\text{Pb}(\gamma, n)$ at $\theta_{\text{lab}} = 55^\circ$. The mean incident photon energy is 23.46 MeV. The time scale in this figure is about 0.5 ns/channel. The arrows denote typical energies relating to the neutron spectrum.

The efficiency of the neutron detector as a function of neutron energy was calculated for various thresholds by a modified version of the Monte Carlo code developed by Stanton.¹² The performance of the program was checked by comparing the calculated efficiencies with those reported in Ref. 13 for an NE-213 liquid scintillator, 12 cm in diameter and 5.7 cm thick. The code reproduced the experimental efficiencies within a few percent.

Overall uncertainties in the absolute cross section were estimated to be $\pm 40\%$, and were mainly due to uncertainties in the neutron counter efficiency and in the attenuation of the γ and neutron flux. The uncertainties in the measured asymmetries (typically 10%) were much smaller than those for the absolute cross sections because of the cancellations which occur between forward and backward

measurements.

Possible spurious asymmetries of the system and systematic errors in the data reduction procedure were investigated by measuring the known asymmetries of the $^{16}\text{O}(\gamma, n_0)^{15}\text{O}$ reaction¹⁴ in the gamma energy range of 20–26 MeV. For this measurement it was necessary to lower the threshold for the neutron counter to 1.0 MeV in terms of the effective electron energy. Our results turned out to be in excellent agreement with those of Jury *et al.*¹⁴ Therefore the occurrence of any spurious asymmetries would appear to be negligible. This reaction also gave us good calibrations of the time-of-flight spectra, since for ^{16}O the (γ, n_0) peak is well separated from the (γ, n_1) peak. The uncertainty in the time calibration of the time-of-flight spectra was estimated to be less than ± 0.1 ns.

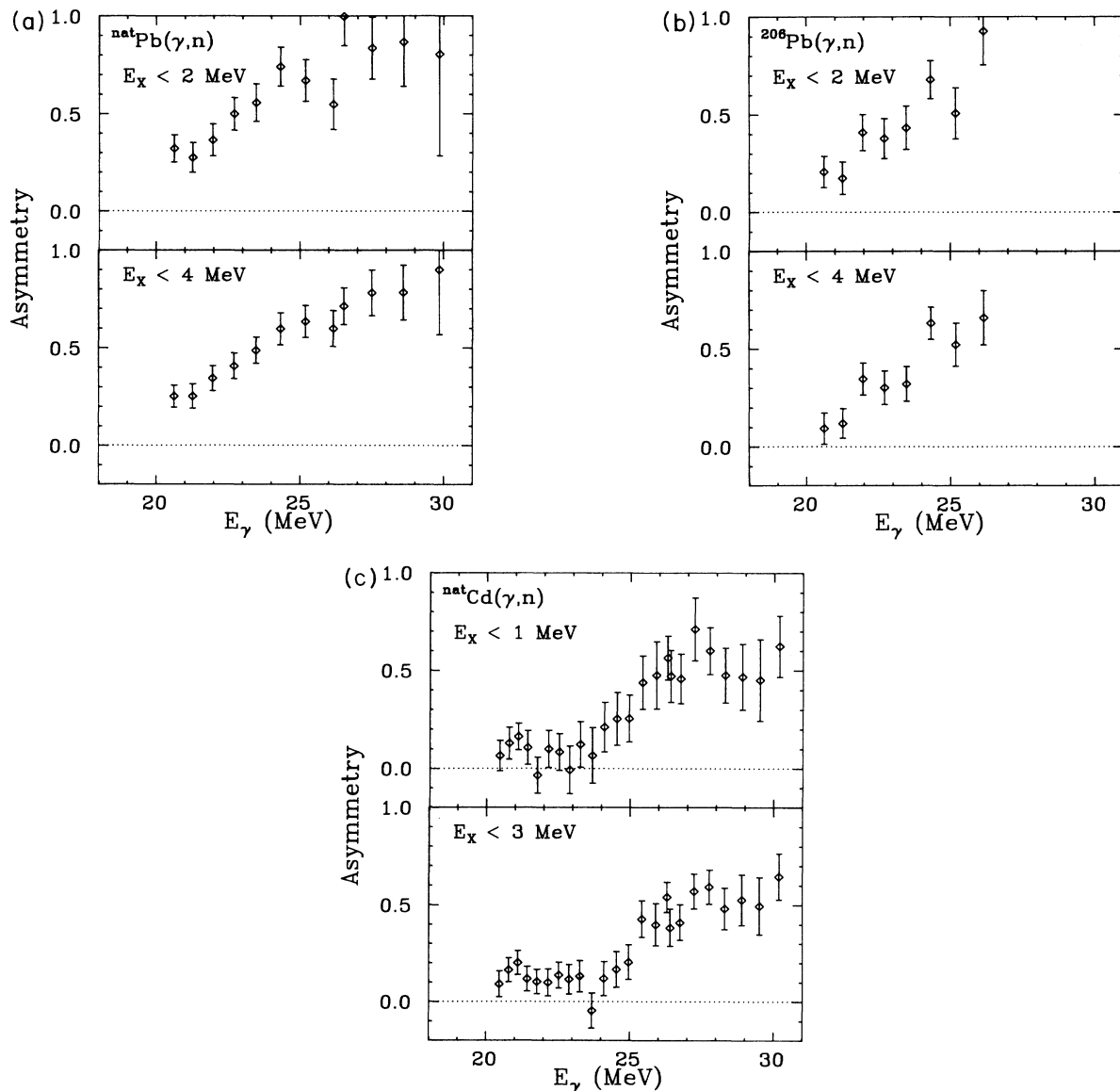


FIG. 2. Asymmetry curves of the (γ, n) reactions for ^{nat}Pb , ^{206}Pb , and ^{nat}Cd targets for residual excitations indicated in the figures. The error bars in the figures reflect only the statistical uncertainties.

III. EXPERIMENTAL RESULTS

The measured asymmetries integrated over an interval of emitted neutron energies are shown in Fig. 2 as a function of photon energy. The neutron energy interval in terms of the excitation energy of the residual nucleus for the most abundant isotope is indicated in the figures. In the case of $^{\text{nat}}\text{Pb}$ the isotope ^{208}Pb has a 52% abundance and the isotopes ^{206}Pb and ^{207}Pb each have abundances of about one-quarter. In the case of $^{\text{nat}}\text{Cd}$ the isotope ^{114}Cd is the most abundant (29%), but the other isotopes $^{110,111,112,113,116}\text{Cd}$ also have fairly large abundances. Since ^{208}Pb and ^{114}Cd do not have the lowest neutron binding energies among the Pb and Cd isotopes, the low-excitation-energy end of the acceptance gate was set so that the yields from the ground states of all isotopes were included.

The asymmetries seem to have a slight dependence on the energy range over which the neutron spectra were integrated, but the statistical errors obscure this dependence. The data for the enriched ^{206}Pb target agree within the statistics with those for natural lead. This fact is consistent with the view that the asymmetry relates to collective modes of nuclear excitation in which finer details of nuclear structure are unimportant.

The asymmetry for $^{\text{nat}}\text{Pb}(\gamma, n)$ changes more slowly with photon energy than that observed earlier in the $^{208}\text{Pb}(n, \gamma_0)$ reaction.⁸ However, the two asymmetry curves are similar in that the asymmetry changes from a small value to a large one near the energy where the isovector $E2$ giant resonance is expected to lie. The asymmetry pattern for $^{\text{nat}}\text{Cd}$ is similar to that for $^{\text{nat}}\text{Pb}$, but the transition region is about 4 MeV higher, consistent with the expected $A^{-1/3}$ dependence for the location of giant resonances in heavy nuclei.

The cross section ratios between the 90° measurement

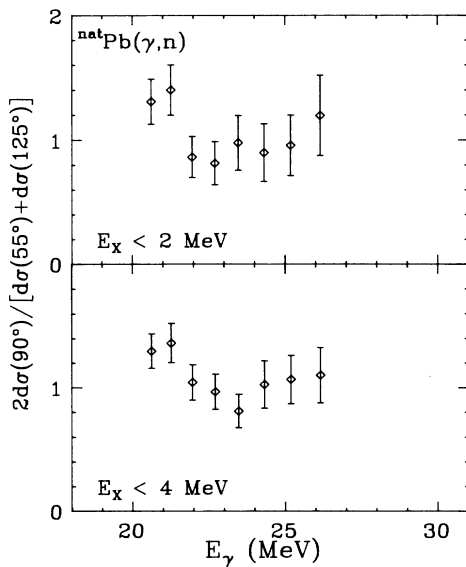


FIG. 3. Ratios between the cross sections at 90° and the average of those at 55° and 125° for the $^{\text{nat}}\text{Pb}(\gamma, n)$ reaction. The residual excitations are indicated in the figures.

and the average of the 55° and 125° measurements for the $^{\text{nat}}\text{Pb}(\gamma, n)$ reaction are shown in Fig. 3. Even though the data do not have good statistical accuracy, these ratios show a definite dip in their values around $E_\gamma = 23$ MeV. This suggests that the ratio of even to odd parity absorption is increasing at that energy. This is consistent with ascribing the observed asymmetry to the onset of the IVQ. The excitation functions of the cross section to the low ly-

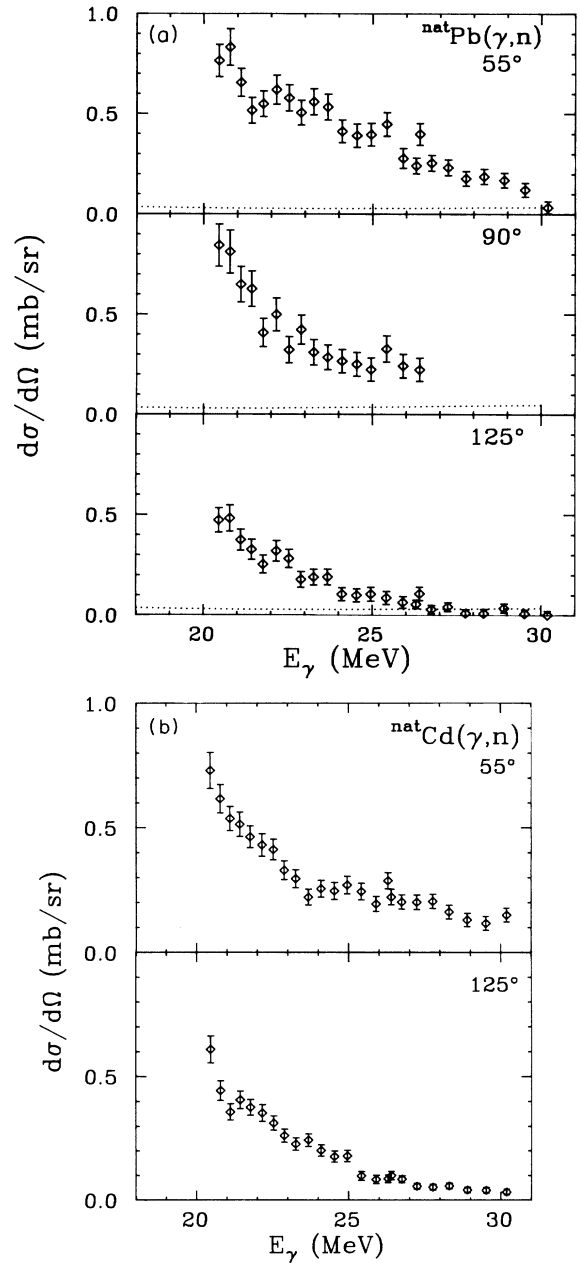


FIG. 4. Cross sections of the (γ, n) reactions for $^{\text{nat}}\text{Pb}$ and $^{\text{nat}}\text{Cd}$ targets at the angles indicated in the figures. The residual excitations are between 0 and 4 MeV for the $^{\text{nat}}\text{Pb}$ target and between 0 and 3 MeV for the $^{\text{nat}}\text{Cd}$ target. The dotted lines in panel (a) are the expected direct process contributions calculated using the DSD model (see Sec. IV C).

ing residual states do not, however, show a noticeable increase in the energy region where the asymmetry changes and where we expect the IVQ to lie. (See Fig. 4.)

IV. DISCUSSION OF RESULTS

This discussion is divided into four parts. It begins with a general treatment of the relation between the measured quantities (cross sections and asymmetries) and the odd and even parity amplitudes upon which these quantities depend. The second part of the discussion is a semiclassical treatment of the asymmetry in which it is assumed, for simplicity, that the dependence of the asymmetry on photon energy is much the same for all residual states. By expressing the odd and even amplitudes in terms of the strength functions for nuclear excitations of different multiplicities, it becomes straightforward, using this model, to estimate the sensitivities of the observed asymmetries and cross sections to the parameters which characterize the relevant giant resonances. In the third part of the discussion we go through the details of a calculation of the expected results using the so-called direct-semidirect (DSD) model for radiative capture reactions¹⁵ along with the principle of detailed balance. The fourth and final part of the discussion compares the DSD analysis of the results with that of the semiclassical description.

A. The asymmetry and the cross section expressed in terms of amplitudes

The data from our measurements provide three independent pieces of information at each excitation energy: (1) a measured fore-aft asymmetry for neutrons which leave the residual nucleus in its lowest few MeV of excitation, (2) some values for the ratio of the 90° yield for these neutrons to their average yield at 55° and 125°, and (3) a measured total cross section for this group of neutrons. We consider emissions to a band of residual excitations because the experimental neutron energy resolution was insufficient to distinguish between individual final states and because it then makes more sense to average over a broad band of final states than to run a risk of biased sampling over only a few final states in a narrow band.

We begin by deriving general expressions for the asymmetry and cross section for a typical residual neutron-hole state for which parity, spin and spin orientation are specified. Let us assume, for the moment, that this state has even parity. Since the target is an even-even nucleus, the intermediate state from which the neutron to this state is emitted is a superposition of both odd-parity (due mainly to $E1$ excitation) and even-parity (due to $E2$ excitation) states. The amplitude for this neutron emission can therefore be expressed as the sum for the emissions from the odd and even parity excitations, $A_j^+ \exp(i\phi_j^+) + A_j^- \exp(i\phi_j^-)$. These two terms refer to a specific residual state j , a specific incident photon energy, and the neutron-emission angle 55°, our forward angle. The corresponding amplitude at 125°, our backward angle, is therefore $A_j^+ \exp(i\phi_j^+) - A_j^- \exp(i\phi_j^-)$ since the odd parity neutron wave function changes sign (but not magnitude) be-

tween 55° and 125°, whereas the even parity function does not change at all.

The quantities $(A_j^-)^2$ and $(A_j^+)^2$ at these angles provide a measure of the contribution of state j to the angle-integrated odd and even parity cross sections, respectively, if the coefficients of $P_4(\cos\theta)$ and higher terms in the Legendre-function expansion of the overall angular distribution are negligible. [We are using the fact that $P_2(\cos 55^\circ) \approx 0$.] Under this assumption the contribution to the angle-integrated cross section is therefore

$$\sigma_j = (A_j^-)^2 + (A_j^+)^2. \quad (1)$$

The front-to-back asymmetry α_j can be expressed in terms of the A 's and ϕ 's for the residual state j as

$$\alpha_j = \frac{2A_j^+ A_j^-}{(A_j^+)^2 + (A_j^-)^2} \cos(\phi_j^+ - \phi_j^-). \quad (2)$$

An important feature of this expression is that α_j is symmetric with respect to an interchange of $+$ and $-$. Thus, α_j has the same value for $A_j^+ / A_j^- = \chi$ as for $A_j^+ / A_j^- = \chi^{-1}$. It depends on the ratio of odd to even amplitudes, but not on which is the larger. This feature of Eq. (2) means that we are free to associate A_j^+ with $E2$ excitation and A_j^- with $E1$ excitation in estimating α_j , although (depending on the parity of the residual one-hole state) the correct association may actually be reversed.

The asymmetry, α_{total} , observed in this experiment is that for the sum of final states,

$$\begin{aligned} \alpha_{\text{total}} &= \frac{\sum_j [\sigma_j(55^\circ) - \sigma_j(125^\circ)]}{\sum_j [\sigma_j(55^\circ) + \sigma_j(125^\circ)]} \\ &= \frac{\sum_j \alpha_j [\sigma_j(55^\circ) + \sigma_j(125^\circ)]}{\sum_j [\sigma_j(55^\circ) + \sigma_j(125^\circ)]}, \end{aligned} \quad (3)$$

i.e., α_{total} is the average α_j , where each state is weighted by the cross section to that state. As a result of the aforementioned symmetry of Eq. (2), with respect to the interchange of $+$ and $-$, one may associate the even parity emission amplitudes $A_j^+ \exp(i\phi_j^+)$ with the even ($E2$) excitations, although, for an odd parity j , the corresponding emission would actually be odd parity. Thus if the excitation amplitudes happen to be independent of j , the α_j of (3) will be also, even though the emission amplitudes will differ for j 's of opposite parity.

In terms of the A 's the observed cross section is

$$\begin{aligned} \sigma_{\text{total}} &= \frac{1}{2} \sum_j [\sigma_j(55^\circ) + \sigma_j(125^\circ)] \\ &= \sum_j [(A_j^+)^2 + (A_j^-)^2]. \end{aligned} \quad (4)$$

B. A semiclassical approach

The relations of the cross sections and asymmetries to the underlying odd and even parity amplitudes for individual residual states, as they have been described in Eqs. (1)–(4), are quite general. In this section we will take up a

semiclassical approximation to these relations. The essence of the approximation will be the assumption that the $A_j \exp(i\phi_j)$ are sufficiently the same for different j , but the same parity, to allow us to substitute for them a single "typical" amplitude, $A^- \exp(i\phi^-)$ for the odd parity excitations and $A^+ \exp(i\phi^+)$ for the even ones. This assumption is suggested by the well-established similarity of giant resonances built upon different states. Thus in what follows the measured asymmetry will be expressed in terms of A^- , A^+ , ϕ^- , and ϕ^+ according to Eq. (2) rather than as a sum over the asymmetries for each of the final single-hole states [Eq. (3)]. We must, however, alert the reader at this point that the DSD calculations (subsection C) will suggest that the asymmetries α_j are actually j dependent. Under these circumstances the energy dependence of α_{total} can differ from that of the "typical" α_j , as we shall see in more detail below.

Our object here will be to deduce from the data what we can about the values of the A 's and ϕ 's. In order to extract a value for the amplitude ratio A^+/A^- (or its reciprocal) from the measured asymmetry, it is seen from Eq. (2) that one must provide an estimate for the phase difference $\Delta\phi$ between the odd and even parity excitations. For Pb such an estimate can be made with the least ambiguity in the excitation energy range from 27 to 30 MeV. It is seen from Fig. 2(a) that the measured asymmetry in this region has an average value of about 0.8, which is fairly close to the maximum possible value for an asymmetry, namely unity. It follows that $\cos\Delta\phi$ must lie between 0.8 and 1. This, in turn, implies that the amplitude ratio A^+/A^- lies between $\frac{1}{2}$ and 2. The high value of $\cos\Delta\phi$, i.e., the small difference between odd and even parity phases, suggests that the region $E_\gamma = 27\text{--}30$ MeV lies *above* the even parity resonance since (1) this excitation region is definitely above the $E1$ resonance in Pb, and (2) the phase difference between two resonances tends to be large in the energy range between the resonant energies and small outside of it.

It is not as easy to deduce the amplitude ratios from the asymmetry data in Pb at the lower energies of Fig. 2(a) as it is at the higher energies, because there is then no way to determine the value of $\cos\Delta\phi$ directly from our experiment. The reasonable requirement that $\cos\Delta\phi$ should change smoothly with energy does not provide enough of a constraint to be very helpful.

In order to extract more information from the measurements, it therefore becomes necessary to introduce some preconceptions, some model-dependent assumptions whether one uses the simple semiclassical model, the DSD model (Sec. IV C), or any other model. In the semiclassical model, the odd and even amplitudes for the "typical" final state will be assigned on the basis of known or assumed properties of the nuclear giant resonances. The essential elements in this picture are illustrated by the idealized excitation curves of Fig. 5. It is assumed here that the photoemission proceeds through three resonances, the odd-parity $E1$ resonance and the even-parity $E2$ isoscalar and isovector resonances. We will write the amplitudes for each resonance in Breit-Wigner (BW) form. Although the actual energy dependences are undoubtedly more complicated than the BW dependences, this form

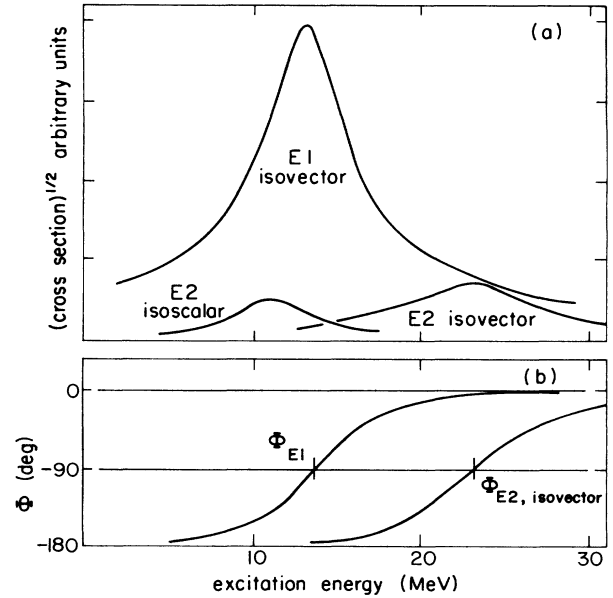


FIG. 5. (a) Idealized giant resonance amplitudes for photon absorption in Pb. (b) Idealized phases for the main odd and even parity amplitudes for the (γ, n) reaction.

has the advantage of being simple while still qualitatively reproducing the main features of the amplitudes. Its use will allow us to make some approximate deductions of values of the $E2$ isovector resonance parameters that match our observations and, perhaps more importantly, will allow us to examine the interplay between the various amplitudes in a convenient and transparent way. The BW amplitudes can be written

$$A_D = \frac{a_D}{\Delta_D + i\Gamma_D/2} \quad (E1), \quad (5)$$

$$A_S = \frac{a_S}{\Delta_S + i\Gamma_S/2} \quad (E2, \text{ isoscalar}), \quad (6)$$

$$A_V = \frac{a_V}{\Delta_V + i\Gamma_V/2} \quad (E2, \text{ isovector}), \quad (7)$$

where $\Delta_D = E_\gamma - E_D^R$, $\Delta_S = E_\gamma - E_S^R$, and $\Delta_V = E_\gamma - E_V^R$, and the energies E^R locate the centers of the respective resonances. The numerators, a , are taken to be positive constants. For a semiclassical model, this corresponds to the correct relative phasing among the three multipoles for the emission of neutrons. (For proton emission, the sign of the $E2$ isoscalar numerator would be reversed.) In the DSD calculations the numerators will be complex. The imaginary parts are generally introduced to reflect couplings to other modes. They will be found to effect the values of the "best fit" resonance parameters.

It is important to appreciate that although each of these resonances is characterized by three parameters (resonance energy, resonance strength, resonance width) the problem of explaining the observed asymmetry as a function of photon energy is not really a nine-parameter problem. It is more nearly a four parameter problem. We are most interested in determining the relatively unknown parameters

E_V^R, Γ_V and the ratio a_V/a_D which characterize the $E2$ isovector resonance. The fourth somewhat uncertain parameter is a_S/a_D , the ratio of the $E2$ isoscalar to the $E1$ amplitude. For the latter ratio it is the mean magnitude of two amplitudes, (5) and (6), in the energy region of interest ($E_\gamma = 20\text{--}30$ MeV) that mainly matters. This is because the resonance energies for these excitations lie far below the region of interest.^{16,17} Their phases are therefore relatively unambiguous and their amplitudes must be changing relatively slowly with energy.

It is reasonable to wonder whether any model restricted to the resonance amplitudes (5)–(7) is general enough. There are other possible amplitudes which are not included in these expressions:

1. Direct amplitudes

It should be recalled that any direct $E\lambda$ amplitude ($\lambda > 1$) is negligible for (γ, n) reactions⁷ because the neutron is uncharged. Any direct $E1$ amplitude would be close in phase to the resonant $E1$ amplitude, and because the DSD calculations show that the direct $E1$ amplitude is small and changing slowly with energy, we consider that (5) can reasonably be considered to represent the sum of the direct and resonant $E1$ amplitudes.

2. Other multipole modes

In the same spirit one should probably think of the $E1$ isovector and $E2$ isoscalar amplitudes as standing in for all odd- and even-parity excitations, respectively, which are nonresonant in the 20–30 MeV range. There may be, for example, a small contribution from $E3$ (Ref. 15) as well as some $M1$ contribution. The only amplitude which we assume to be resonant, between 20 and 30 MeV, and therefore rapidly changing in phase and in magnitude in that energy span, is the $E2$ isovector amplitude. The observed drop, in this energy interval, of the ratio of the 90° cross section to the average of those at 55° and 125° (Fig. 3) shows that it is even rather than odd parity that is growing in, in support of this assumption.

3. Statistical emission

Any statistical decay would reduce the observed asymmetry. Indeed, no asymmetry at all is seen in ^{208}Pb up to 16 MeV.¹⁶ The contribution of statistical neutron emission was estimated using the evaporation code PACE (Ref. 17) with standard parameters. At 20 MeV the cross section for such emission to the lowest 4 MeV of excitation is calculated to be less than 1% of the observed cross section. Beyond this energy it falls off with increasing E_γ as $\exp(-E_\gamma/T)$, where T is the nuclear temperature (about 1 MeV in our energy range). The contribution of statistical neutron emission should therefore be negligible at all energies of this experiment, even considering the uncertainty in the evaporation calculation.

Our first application of the semi-classical model was to see whether the amplitudes of the form in Eqs. (5)–(7), when used in Eq. (2), would give asymmetries close to those observed when the resonance strengths were chosen to be in accord with the energy-weighted sum rules.¹⁸ The

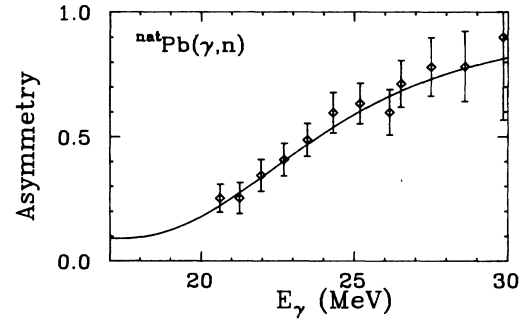


FIG. 6. The asymmetry curve for the $^{nat}\text{Pb}(\gamma, n)$ fitted by the semiclassical model (see text) together with the experimental data. The residual excitations are between 0 and 4 MeV.

numerators in the resonant amplitudes are actually proportional to the product of two factors. One factor is proportional to the square root of the sum-rule strength for photoabsorption for the particular multipole. The second factor is the square root of the average branching ratio for neutron emission to one of the final states of this experiment. At the high energies involved, it is reasonable to assume that this average branching ratio is much the same for all of the multipoles in Eqs. (5)–(7). This second factor was consequently ignored in estimating the asymmetries since the asymmetries depend only upon amplitude ratios.

Thus the three parameters for the odd-parity amplitude were assigned to be in accord with the accepted values for the giant dipole resonance.¹⁹ Corresponding values for the $E2$ isoscalar resonance²⁰ were used for one of the two even-parity amplitudes. The parameters for the $E2$ isovector amplitude, the remaining contributor to even parity, were chosen to be consistent with the $E2$ sum rule and to make the computed asymmetry curve match the observed one (Fig. 6). All of these parameters are listed in Table I.

It was found in this way that a rather good match to the asymmetry curve could be obtained for values of the $E2$ isovector resonance energy and strength which were close to those expected and for a width that was a lot wider than expected. Although it was gratifying to find parameters that gave a good fit to the asymmetry data, we must not accept the implied $E2$ isovector parameters without further scrutiny, as we shall see below.

A number of additional exercises were carried out to explore the sensitivity of the calculated asymmetry to the

TABLE I. Giant resonance parameters used in the semiclassical model.

	$E1^a$	$E2$ isoscalar ^b	$E2$ isovector ^c
Width (MeV)	4.0	3.0	16.0
Energy (MeV)	13.5	10.5	21.5
Strength a^d	(1.0)	0.08	0.53

^aFrom Ref. 19.

^bFrom Ref. 20.

^cFrom fit to asymmetry curve.

^dNumerator in Eqs. (5)–(7).

various resonance parameters. The results are shown in Fig. 7.

It is seen that either an increase or a decrease in the $E2$ isovector cross section (or amplitude) reduces the predicted asymmetry at the higher energies. The fact that the asymmetry is near its maximum possible value implies, as we have already noted, that A^+ must, for these energies, be comparable to A^- since the asymmetry peaks when $A^+/A^- = 1$ [Eq. (2)]. Near this maximum, the asymmetry becomes relatively insensitive to the assumed mag-

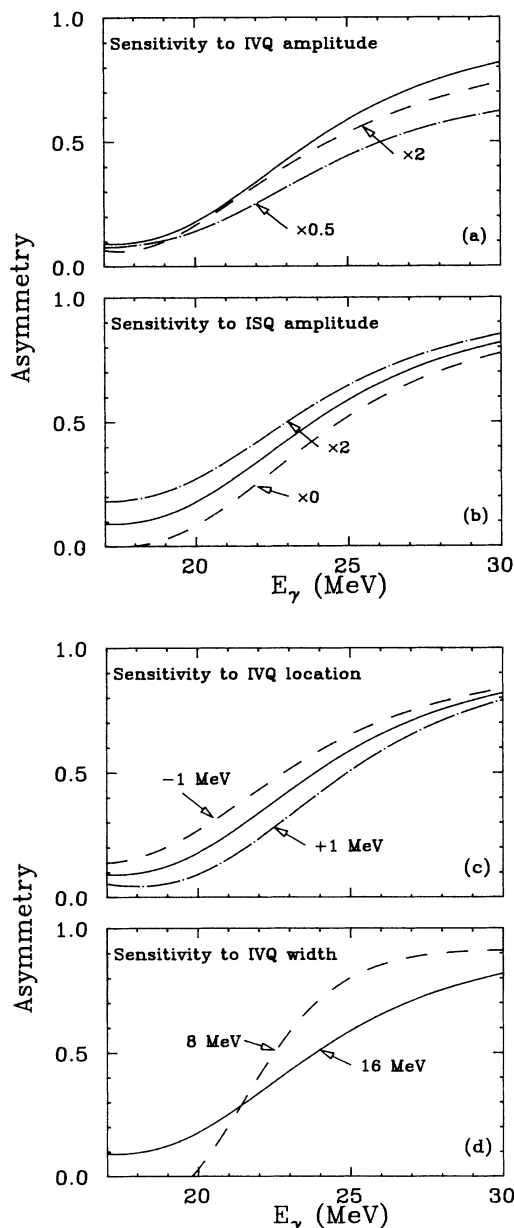


FIG. 7. Sensitivity of the asymmetry to the values of the four critical resonance parameters defined in the text. The solid curve in each figure is the fitted curve of Fig. 6. [Both curves in panel (d) are for the same integrated strength for the IVQ resonance.]

nitude of the $E2$ isovector cross section. The dashed and dotted-dashed solid curves in Fig. 7(a) correspond to $E2$ cross sections which are four times higher and 4 times lower than the best-fit curve.

The $E2$ isoscalar amplitude in the region of 20–30 MeV is rather weak since the resonance lies near 10 MeV and is quite narrow.²⁰ Nonetheless, because it is its amplitude rather than its intensity which matters, the isoscalar resonance plays a role. It slightly increases ϕ^+ , the positive parity phase. This tends to close the gap between ϕ^+ and ϕ^- and therefore to increase the asymmetry, as the curve in Fig. 7(b) shows.

It is also seen from Figs. 7(b) and 7(c) that an increase in the assumed amount of $E2$ isoscalar resonance can be offset by a shift of the $E2$ isovector resonance to a higher energy. In particular a factor of 2 increase in the isoscalar amplitude from the originally assumed value can be compensated for by an upward shift in the isovector resonance energy of about an MeV.

There is a warning in the foregoing result. Any effect which introduces an appreciable phase shift between negative and positive parity amplitudes will shift the asymmetry curve. To provide a scale for these effects we note that the doubling of the isoscalar amplitude in Fig. 7(b) changes ϕ^+ by values of only 3° – 10° (between 20 and 30 MeV). There can be sources of phase shift at least as large as this from effects which have been completely ignored in the semiclassical model. These are discussed in Sec. IV D, where the results deduced using this model are compared with those using the DSD model.

The width of the $E2$ isovector resonance which was needed to obtain the fit in Fig. 6 is enormously large compared to that of the dipole isovector resonance (Table I). Even though the $E2$ isovector width is certainly expected to be larger than the $E1$ width since both the escape and spreading widths increase with the energy of a giant resonance, an increase as large as that in Table I is unexpected. Figure 7(d) shows that a significantly narrower assumed width will not fit the data.

One might wonder whether the difficulty here stems from having assumed a wrong energy dependence for A^+ or A^- , but it is easy to demonstrate that even large changes in the relative sizes of the A 's lead to only small effects on the asymmetry curve. For example, if the even parity cross section is held fixed and the odd parity cross section is doubled at 20 MeV and then allowed to change gradually until it is only half of the best-fit cross section at 30 MeV, the asymmetries remain within 0.03 of those in the "best-fit" curve throughout the energy range. The effect is only slightly larger if it is the odd parity amplitude that is kept fixed and the even parity cross section is changed by the factor of 4 between 20 and 30 MeV. The reason for this remarkable insensitivity of the asymmetry to the cross sections is that at the higher energies where $\chi = A^+/A^-$ approaches unity, the asymmetry becomes stationary as a function of χ . At lower energies where χ and the asymmetry are both small, even large percentage changes in the asymmetry correspond to small absolute changes. As a result, the overall shape of the curve is hardly affected.

A comparison of Figs. 7(a) and 7(d) suggests that if one

combines a narrow IVQ width with a reduction of the IVQ strength from the sum-rule value, the resulting asymmetry would possibly give as good a fit to the data as that obtained with the full sum-rule strength and the 16 MeV width (the IVQ parameters in Fig. 6). This is indeed the case, as the asymmetry curve for half the sum rule strength and a width of 12 MeV is virtually indistinguishable from the curve in Fig. 6. It becomes difficult, however, to fit the data for widths smaller than 12 MeV. Thus the analysis of the data using the semiclassical model suggests that the IVQ resonance is substantially wider than the IVD resonance. A possible reason that this model gives so large a width is discussed in Sec. IVD below (after we have had a chance to examine the corresponding analysis using the DSD model).

We now turn briefly to the second major quantity measured in this experiment, the cross section for the (γ, n) reaction (to the particular residual-energy interval) as a function of photon energy. In contrast to the fore-aft asymmetry, the cross section depends on the A 's and not at all on the ϕ 's. Thus the fitting of the asymmetries and of the cross section data are essentially decoupled.

The cross section calculated from the amplitudes in Table I [see Eq. (1)] is found to decrease by a factor of 3 between 21 and 29 MeV, whereas the experimental cross section falls by more nearly a factor of 6 in the same energy interval. This sort of discrepancy is not altogether surprising since the branching ratios for neutron decay to the low lying levels in Pb have not been included in the semiclassical calculation. Although, as we have noted, these ratios should play only a minor role in the asymmetries, they enter directly in the estimates of the cross sections. Since they necessarily fall off as the energy goes up and new emission channels open, one must expect the actual cross section to fall off faster than that of a calculation where the effect of branching was neglected.

No attempt has been made to use the semiclassical model to fit the asymmetries or cross sections for our other target, ^{nat}Cd . The observed cross section in ^{nat}Cd falls off at about the same rate between 21 and 29 MeV as it does in ^{nat}Pb . The asymmetry curve in Cd is shifted to higher photon energy by an amount consistent with an $A^{-1/3}$ dependence for the location of the isovector resonance and it seems to level off at a somewhat lower value for the maximum asymmetry. This should be checked by extending the measurements for both Pb and Cd to higher energies.

C. The DSD model

The semiclassical model which we have used up to this point to discuss the data does not include a number of considerations which affect the magnitudes and phases of the interfering amplitudes in the (γ, n) reaction. These are presumably included in the so-called direct-semidirect (DSD) model,²¹ which, as its name implies, includes direct amplitudes as well as the resonant (semidirect) amplitudes, (5)–(7), of the semiclassical model. The DSD model also treats individual final states one at a time. To compare the results of DSD calculations with our data, we must sum the calculations over the final states which lie in the residual energy interval.

The differential cross sections for the (γ, n) reaction were obtained using detailed balance from calculations made in the inverse direction; i.e., we calculated the matrix elements for neutron capture by a target which is in an excited single-hole state. In order to apply the DSD model to the case of targets with spin, e.g., to targets in an excited state, we followed the prescription of Snover²² in assuming that the semidirect process depends only on the final state parentage to the target ground state plus a single nucleon. The details of this treatment can be found in Ref. 23. Beside this assumption, it was supposed that the optical potential which is used for the ground state calculation also describes the scattering of neutrons by the excited nucleus, and that this optical potential is independent of the spin of the target nucleus. The bound state neutron wave function was calculated using the same geometrical parameters as those for the real part of the optical potential. The depth of the real part of this potential was adjusted to reproduce the binding energy of the neutron. The strength of the spin-orbit force in the bound state problem was the same as in the optical potential. In carrying out our numerical calculations, we used two sets of global optical potentials, one due to Rosen *et al.*²⁴ and the other due to Becchetti and Greenlees.¹¹ Our purpose was to see the sensitivity of the calculations to optical model prescriptions. The explicit values of the optical potential parameters which we used are given in Refs. 24 and 11.

According to the DSD model, the transition amplitude for the neutron capture reaction on spin-zero targets for electric radiation of multipolarity L , circular polarization p ($= \pm 1$), and spin projection s (with the quantization axis in the projectile direction) can be written as

$$T_{Lps}^{nljm} = (C^2 S_{lj})^{1/2} \langle \Phi_{nljm} | \left[d_{Lp}(\mathbf{r}_\gamma, \mathbf{r}) + \sum_{T=0,1} \frac{v_{LpT}(\mathbf{r}_\gamma, \mathbf{r})}{E - E_{LT} + i\Gamma_{LT}/2} \right] | \chi_{1/2s} \rangle. \quad (8)$$

Here, $\chi_{1/2s}$ is the neutron scattering wave function obtained from the optical model, and Φ_{nljm} is the single particle state wave function with quantum numbers n , l , j , and m into which the neutron is captured.^{25,26} The vectors \mathbf{r} and \mathbf{r}_γ denote coordinates for the neutron and photon, respectively. The spectroscopic factor for the final state is denoted $C^2 S_{lj}$. E is the total energy of the system,

while E_{LT} and Γ_{LT} are the position and width of the giant resonance. The subscript T represents the isospin state. For the quadrupole excitations, the isoscalar (ISQ) resonance must be included as well as the isovector (IVQ) resonance, since the isoscalar quadrupole resonance was found to affect the fore-aft asymmetry.²⁷ The term $d_{Lp}(\mathbf{r}_\gamma, \mathbf{r})$ is the single-particle multipole operator for mul-

tipolarity L . The factor $v_{LpT}(\mathbf{r}_\gamma, \mathbf{r})$ is the incident neutron target-nucleus vibration coupling interaction, i.e., the form factor for the inelastic excitation of the collective electric multipole state by the incident neutron. It should be noted that, in order to obtain the correct resonance shape for heavy nuclei in capture reactions, it is usually necessary to introduce a complex form factor for the particle-vibration coupling, with a relatively large imaginary strength.²⁵

In the conventional long wavelength approximation the quantities $d_{Lp}(\mathbf{r}_\gamma, \mathbf{r})$ and $v_{LpT}(\mathbf{r}_\gamma, \mathbf{r})$ can be written as

$$d_{Lp}(\mathbf{r}_\gamma, \mathbf{r}) = \sum C_{Lp}(k) e_L r^L D_{pM}^{L*}(\hat{\mathbf{r}}_\gamma) Y_{LM}^*(\hat{\mathbf{r}}) \quad (9)$$

and

$$v_{LpT}(\mathbf{r}_\gamma, \mathbf{r}) = \sum C_{Lp}(k) e_L h_{LT}(r) D_{pM}^{L*}(\hat{\mathbf{r}}_\gamma) Y_{LM}^*(\hat{\mathbf{r}}), \quad (10)$$

with

$$C_{Lp}(k) = p \left[\frac{2\pi \hbar k c}{V} \right]^{1/2} (-ik)^{L-1} \times \left[\frac{2\pi(2L+1)(L+1)}{L} \right]^{1/2} \frac{1}{(2L+1)!!} \quad (11)$$

and

$$e_L = \left[\frac{-m_n}{m_n + m_t} \right]^L Z_t e. \quad (12)$$

Here, k is the photon wave number and V is the volume enclosed by the surface on which periodic boundary conditions are imposed. The mass of the neutron and target, and the charge of the target, are denoted by m_n , m_t , and Z_t , respectively. We chose the following radial forms for $h_{LT}(r)$:

$$h_{11}(r) = \frac{3N}{A} \frac{\hbar^2}{m_n} \frac{P_{11}}{E_{11}} \frac{1}{\langle r^2 \rangle} r \left[\frac{V_1}{4} f(r) - iW_1 a \frac{dg(r)}{dr} \right], \quad (13)$$

$$h_{20}(r) = 2Z \frac{\hbar^2}{m_n} \frac{P_{20}}{E_{20}} r^2 \left[-\frac{V_0}{r} \frac{df(r)}{dr} \right], \quad (14)$$

$$h_{21}(r) = -10N \frac{\hbar^2}{m_n} \frac{P_{21}}{E_{21}} \frac{\langle r^2 \rangle}{\langle r^4 \rangle} r^2 \left[\frac{V_1}{4} f(r) - iW_1 a \frac{dg(r)}{dr} \right]. \quad (15)$$

These radial forms are essentially the same as those of Ref. 28, but we explicitly include the possibility that only a fraction P_{LT} of the EWSR is exhausted. Here, N , Z ,

and A denote the neutron, charge, and mass numbers of the target, respectively, and $\langle r^\lambda \rangle$ is the mean of the radial coordinate of a nucleon raised to the λ power. The functions $f(r)$ and $g(r)$ are the Woods-Saxon form factors for the real and imaginary parts of the optical potential, respectively, and a is the diffuseness in the function $g(r)$.

Since the photon energies involved in this experiment were quite high, we were concerned that the long wavelength approximation might not be applicable. We therefore made some calculations replacing the $e_L r^L$ factor in the form factors $d_{Lp}(\mathbf{r}_\gamma, \mathbf{r})$ and $v_{LpT}(\mathbf{r}_\gamma, \mathbf{r})$ with

$$e Z_t \frac{(2L+1)!!}{(L+1)k^L} \frac{\partial}{\partial R} [R j_L(kR)], \quad (16)$$

where $R = -m_n r / (m_n + m_t)$. This factor is a more accurate expression for the electric multipole moment. Those calculations showed that this modification only changed the cross section by 7% or less around $E_\gamma = 30$ MeV. There were no noticeable changes in the asymmetry curves. Nevertheless, we use the full form rather than the long wavelength form throughout this paper.

Before applying this formalism to the present (γ, n) experiment, we calculated the asymmetry for the capture reaction $^{208}\text{Pb}(n, \gamma_0)$ in order to compare it with the available data.⁸ The spectroscopic factor of the ^{209}Pb ground state was set equal to 1, and the $\langle r^2 \rangle$ and $\langle r^4 \rangle$ values, 30.5 fm² and 1161 fm⁴, for the ^{208}Pb , were taken from electron scattering data.²⁹ For the coupling strength parameters V_1 and W_1 we used the values suggested by Potokar *et al.*²⁵ for the IVD, namely $V_1 = 75$ MeV and $W_1 = 125$ MeV for the Rosen potential, and $V_1 = 60$ MeV and $W_1 = 120$ MeV for the Becchetti-Greenlees potential. The isoscalar coupling constant V_0 was assumed to be -50 MeV. The resonance parameters used for the calculation are given in Table II. They are essentially empirical values,^{19,20} except for the parameters for the IVQ, which we adjusted to give the best simultaneous reproduction of the asymmetry curves for both the $^{208}\text{Pb}(n, \gamma_0)$ and $^{nat}\text{Pb}(\gamma, n)$ reactions. The cross sections of the $^{208}\text{Pb}(n, \gamma_0)$ reaction in the energy range $E_n = 6-15$ MeV (Ref. 30) are well reproduced by a DSD calculation, as Potokar *et al.*²⁵ have already reported. The asymmetry curve measured by Drake *et al.*⁸ is also reasonably well explained (Fig. 8), but it is seen that at the high energy end of the calculation the two optical potentials predict quite different results. The rapid rise of the asymmetry clearly comes from the interference between the IVD and the IVQ. Without the IVQ, we can get only a slow and small increase in the asymmetry. The inclusion of the ISQ seems to be essential to explain the absence of a negative asymmetry below the IVQ resonance, as has been already pointed out by Longo *et al.*³¹

TABLE II. Giant resonance parameters used in the DSD calculation.^a

Target	E_D	Γ_D	P_{11} (%)	E_V	Γ_V	P_{21} (%)	E_S	Γ_S	P_{20} (%)
Pb	13.42	4.05	117	23.50	6.00	40	10.50	2.80	95
Cd	15.8	6.3	106	26.50	7.00	50	13.20	3.30	84

^aEnergies in MeV.

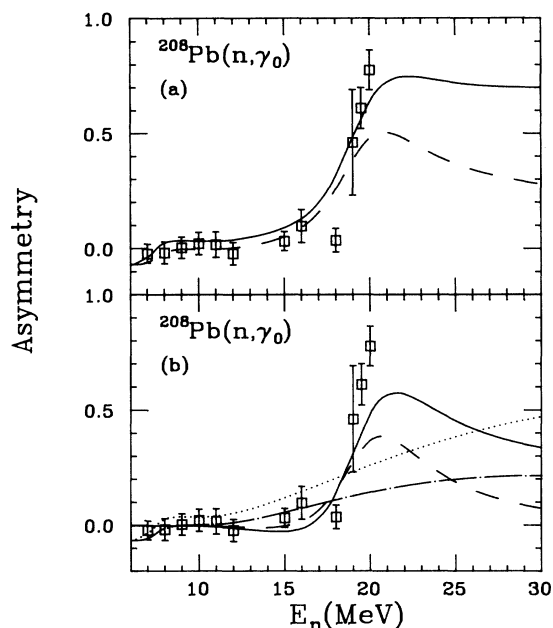


FIG. 8. Comparison of the DSD model prediction for the $^{208}\text{Pb}(n, \gamma_0)$ reaction to the experimental data (from Ref. 8). (a) The solid and dashed curves are predictions of the DSD model including the ISQ, IVD, and IVQ, and using the optical potentials from Refs. 24 and 11, respectively. In panel (b) the solid and dashed curves are the DSD model prediction including only the IVD and IVQ, and the dotted and dotted-dashed curves are the predictions including only the ISQ and IVD. The resonance parameters are listed in Table II.

Although the (γ, n) target in the experiment was ^{nat}Pb , the calculations were carried out for only ^{208}Pb since the isotope dependence of the (γ, n) reaction at these energies is small. Candidates for the final states of the $^{208}\text{Pb}(\gamma, n)$ reaction are the single-hole states, which are listed in Table III. The spectroscopic factors for these states are taken from Ref. 32. They are all reasonably close to maximum possible values. The $\langle r^2 \rangle$ and $\langle r^4 \rangle$ values for ^{207}Pb were 30.4 fm^2 and 1155 fm^4 , respectively, again obtained from electron scattering data.²⁹ All other parameters were taken to be the same as in the calculation of $^{208}\text{Pb}(n, \gamma_0)$.

In Fig. 4(a) we compare the calculated cross section for only a direct (nonresonant) process (dotted line) with the measured one for ^{nat}Pb . It is clear that the direct process alone gives a serious underestimate of the observed cross

TABLE III. Neutron hole states in ^{207}Pb .^a

E_x (MeV)	Spin	C^2S_{ij}
0.0	$3p_{1/2}$	2.3
0.572	$2f_{5/2}$	6.2
0.899	$3p_{3/2}$	7.0
1.629	$1i_{13/2}$	12.0
2.334	$2f_{7/2}$	7.3
3.415	$1h_{9/2}$	6.9

^aFrom Ref. 32.

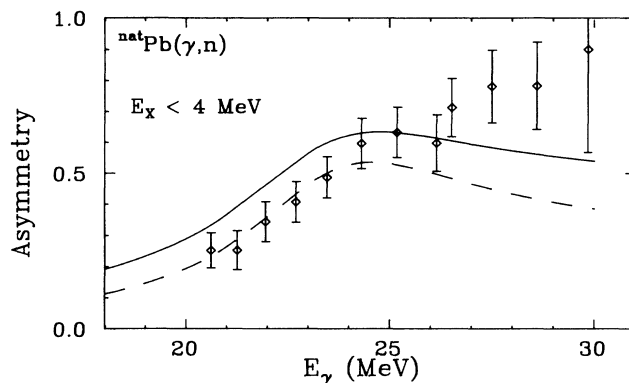


FIG. 9. Asymmetry curves for the $^{nat}\text{Pb}(\gamma, n)$ reaction predicted by the DSD model with the resonance parameters (Table II) based on available data and the assumption $E_{IVQ} = 23.5 \text{ MeV}$ and $\Gamma_{IVQ} = 6 \text{ MeV}$ shown together with the experimental data. Solid and dashed curves are the results with the optical potentials from Refs. 24 and 11, respectively.

section. To account for the latter it is necessary to involve a semidirect, i.e., a resonant process.

The results of the full DSD calculation summed over several final states are shown along with the data in Figs. 9–11. For reference the asymmetry curves and the excitation functions of the cross sections for each of these final states are shown in Figs. 12(a) and 12(b). It is seen that there is an appreciable final state dependence especially for final states which have angular momenta close to the grazing angular momentum ($\approx 7\hbar$). The general behavior of the calculated averaged asymmetries (weighted by the cross section to each individual state) and cross section ratios seem to reproduce the trend of the data reasonably well. Above $E_\gamma = 26 \text{ MeV}$ there are, however, rather large discrepancies between the DSD prediction and the data for the asymmetry; i.e., the measured asymmetry keeps increasing, while the calculated asymmetry begins to decrease as E_γ increases. The inclusion of an

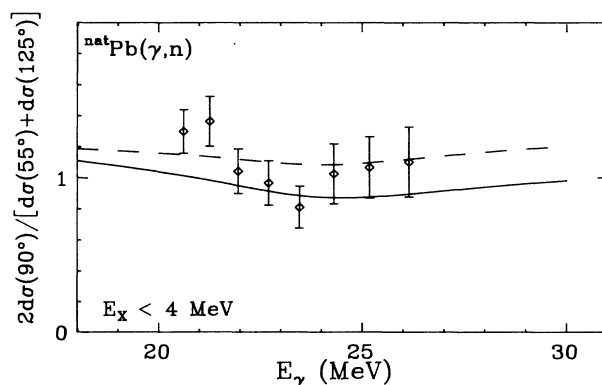


FIG. 10. Measured and predicted cross section ratios between 90° and the average of those at 55° and 125° for the $^{nat}\text{Pb}(\gamma, n)$ reaction. Solid and dashed curves are the results with parameters referred to in Fig. 9.

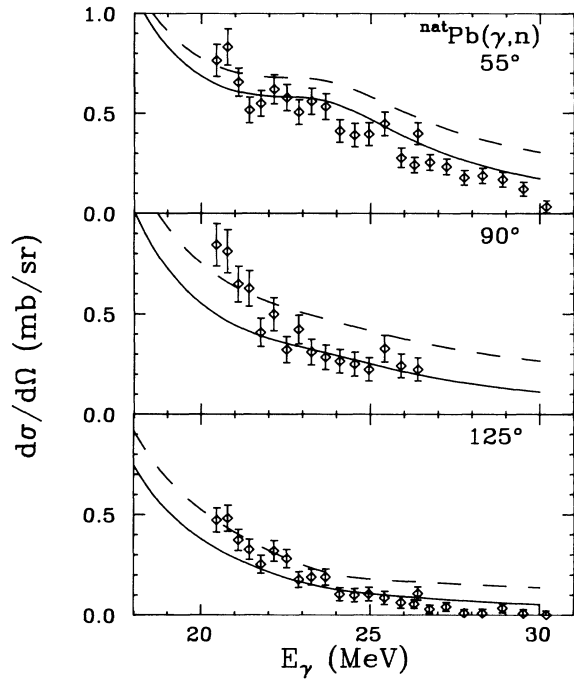


FIG. 11. Predicted cross section for the $^{nat}\text{Pb}(\gamma,n)$ reaction at 55° , 90° , and 125° together with the data. Solid and dashed curves are the results with the parameters referred to in Fig. 9. The residual excitations are between 0 and 4 MeV.

isovector $E3$ giant resonance which is predicted around $E_x = 33$ MeV with a strength of the 58% of the energy-weighted sum rule³³ does not improve this discrepancy at all. Perhaps the easiest way to obtain better agreement would be to introduce extra even-parity strength above $E_\gamma = 26$ MeV or to widen the isovector $E2$ resonance in order to give larger even-parity strength on the high energy tail of the IVQ.

The energy dependence of the cross section for $^{208}\text{Pb}(\gamma,n)$ presented another problem. The parameters (Table II) for the best overall fit to (γ,n) and to (n,γ_0) on ^{208}Pb put the IVQ width at 6 MeV and the fraction of the sum rule strength in the resonance at 40%. Any increase in strength or decrease in width enlarges the bump (seen at 55° in the calculated cross section) which appears around the center of the IVQ resonance (Fig. 11). Since no such bump is observed in the experimental data, these data require an IVQ strength distribution that is more spread out than that deduced from an analysis of inelastic electron scattering.²⁰

For the $^{nat}\text{Cd}(\gamma,n)$ reaction the DSD calculation of the asymmetry is more complicated than for Pb. The distribution of single particle strength among the low-lying states in Cd is less obvious since Cd is far from a closed shell. According to the quasiparticle model, for an even-even parent nucleus in its $J=0$ ground state, the population of single-hole states with angular momentum j is given by the spectroscopic factor

$$C^2S_{lj} = V_j^2(2j+1), \quad (17)$$

where V_j^2 is the occupation number. Again, we treat only the most abundant isotope, i.e., ^{114}Cd , in the model calculation. The V_j^2 values and the relative single quasiparticle energies E_j for the ^{114}Cd nucleus were obtained from Ref. 34. The absolute locations of the neutron single quasiparticle states were determined by assuming that the $3s_{1/2}$ state is at $E_x(^{113}\text{Cd}) = 214$ keV, which is close to the center of gravity excitation energy for $j = \frac{1}{2}$ states excited by the $^{114}\text{Cd}(d,t)^{113}\text{Cd}$ reaction.³⁴ The unknown V_j^2 value for the $1g_{7/2}$ state in ^{114}Cd was assumed to be the same as in ^{112}Cd . These values are summarized in Table IV. The resonance parameters^{35,36} used for the calculation are given in Table II. Since the ISQ in the ^{114}Cd is not well

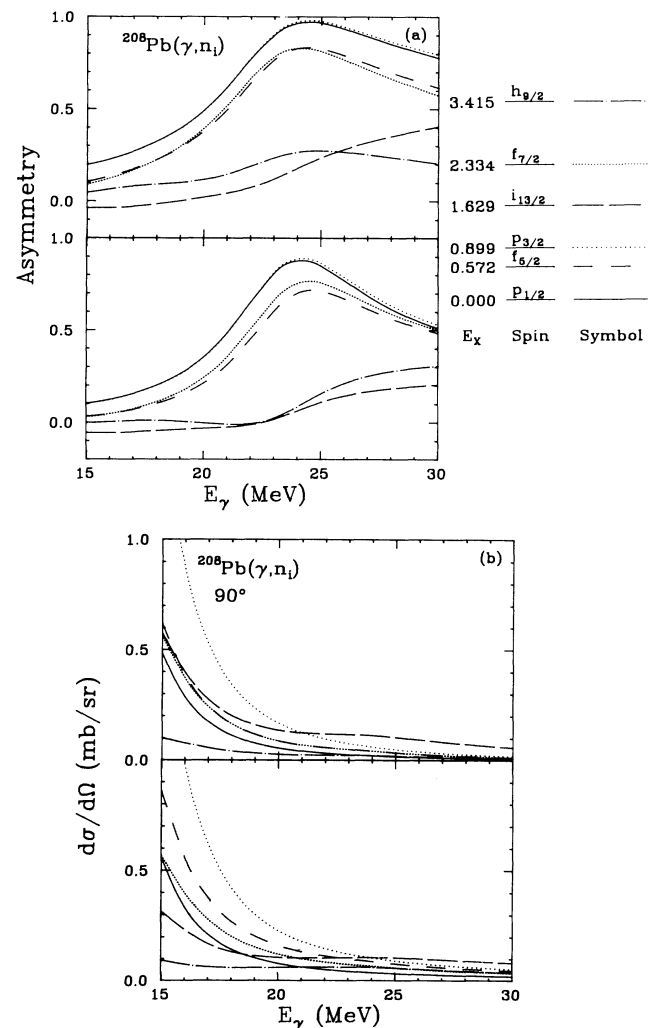


FIG. 12. Final state dependence (a) of the asymmetry and (b) of the cross section at 90° for the $^{208}\text{Pb}(\gamma,n_i)$ reaction calculated with the DSD model. Top and bottom parts correspond to the results with the optical potentials from Refs. 24 and 11, respectively, and the resonance parameters referred to in Fig. 9. Solid, dashed, dotted, long dashed, fine dotted, and dotted-dashed curves correspond to the $3p_{1/2}$, $2f_{5/2}$, $3p_{3/2}$, $1i_{13/2}$, $2f_{7/2}$, and $1h_{9/2}$ states, respectively.

TABLE IV. Occupation number V_j^2 and single quasiparticle energy E_j for ^{114}Cd .

State	E_j (keV)	V_j^2
$3s_{1/2}$	214	0.27
$2d_{1/2}$	445	0.25
$2d_{5/2}$	700	0.78
$1g_{7/2}$	480	0.84
$1h_{11/2}$	180	0.35

known, we adopted the empirical resonance parameters for ^{116}Sn .³⁶ For $\langle r^2 \rangle$ and $\langle r^4 \rangle$ values for ^{113}Cd we used 21.4 fm^2 and 577.8 fm^4 , respectively.²⁹ Since the coupling strengths V_1 and W_1 for $^{\text{nat}}\text{Cd}$ have not been investigated previously, we treat them the free parameters adjusted to fit the measured absolute cross sections while keeping the ratio between them the same as for the $^{\text{nat}}\text{Pb}(\gamma, n)$ reaction. The final values for $^{\text{nat}}\text{Cd}$ are then $V_1 = 54 \text{ MeV}$ and $W_1 = 91 \text{ MeV}$ for the Rosen potential, and $V_1 = 41 \text{ MeV}$ and $W_1 = 82 \text{ MeV}$ for the Becchetti-Greenlees potential. In Fig. 13 the result for the asymmetry is compared with the experimental data integrated over the range of residual excitation energies up to 3 MeV. This range is probably large enough to include all fragmented quasiparticle states. The position and the width of the IVQ were roughly adjusted to get fair agreement with the data.

Despite the crudeness of the DSD calculations, we find, as we did for Pb, that the calculation can qualitatively ac-

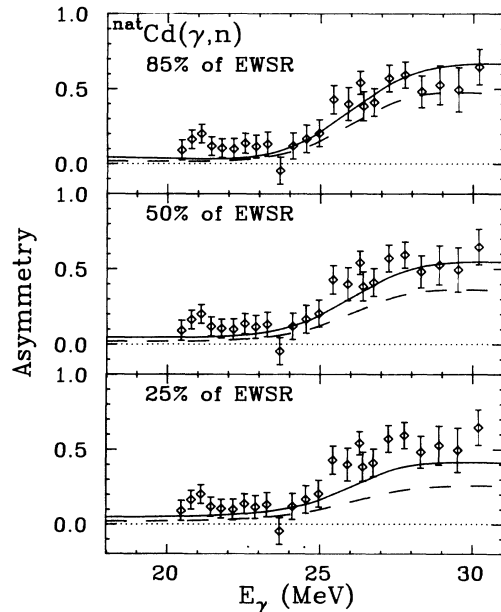


FIG. 13. Asymmetry curves for the $^{\text{nat}}\text{Cd}(\gamma, n)$ reaction predicted by the DSD model together with the experimental data. The residual excitations are between 0 and 3 MeV. Solid and dashed curves are the results with the optical potentials from Refs. 24 and 11, respectively. Resonance parameters are listed in Table II.

count for the observed Cd asymmetry curve. The strength of the IVQ resonance required for a best fit in Cd is again about half the sum-rule strength (see Figs. 13 and 14). The IVQ strength appears to be more widely distributed than the analysis of the (e, e') data suggests.

D. Comparison of the two models

In the earlier parts of this section we have examined our experimental results (especially those for $^{\text{nat}}\text{Pb}$) using

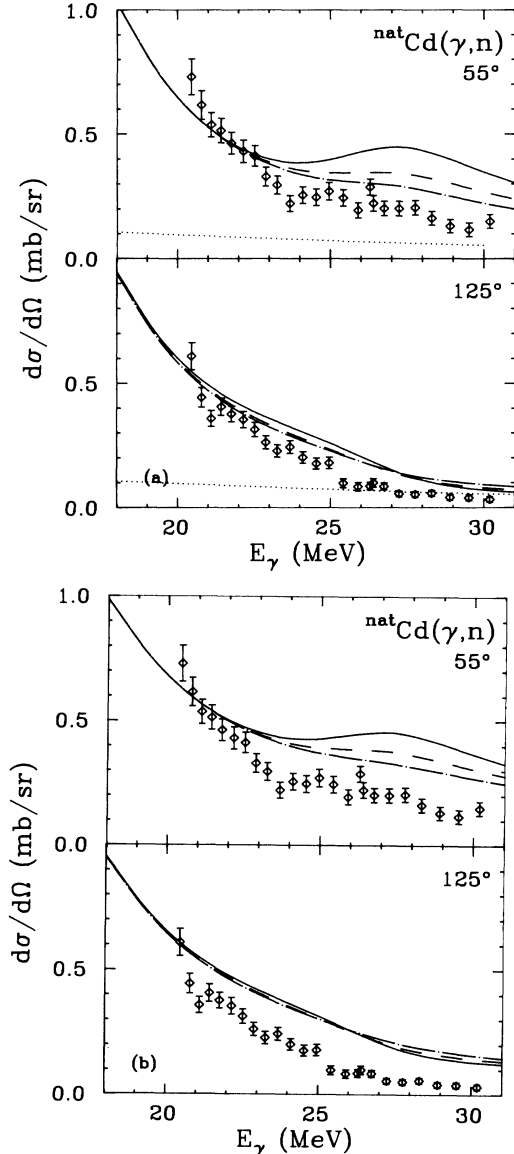


FIG. 14. Cross section for the $^{\text{nat}}\text{Cd}(\gamma, n)$ reaction predicted by the DSD model together with the experimental data. The residual excitations are between 0 and 3 MeV. (a) and (b) are the results with the optical potentials from Refs. 24 and 11, respectively. Solid, dashed, and dotted-dashed curves correspond to 85%, 50%, and 25% of the EWSR strength, respectively. The other resonance parameters are listed in Table II. Dotted curves are the calculated direct process contributions.

two theoretical models to determine the values of the parameters which characterize the IVQ resonance.

1. Asymmetry curves

It was found that although the measured asymmetries could be qualitatively reproduced with either a very schematic semiclassical model or with the direct-semidirect model, the sets of resonance parameters deduced from the two models disagreed. The semiclassical model gave a lower energy and a much wider resonance. Some of this disagreement can be accounted for by a close examination of the two models.

a. The location of the IVQ resonance. The DSD model places the IVQ resonance at 23.5 MeV, whereas the semiclassical fit puts it at 21.5 MeV. In both models it is the shape and location of the asymmetry curve that is used to assign the IVQ resonance energy. We have seen that the asymmetry depends mainly on the phase difference between interfering positive and negative parity amplitudes rather than on the magnitudes of these amplitudes. The DSD calculation includes three contributions to the phase of these amplitudes which do not appear in our semiclassical calculation.

(i) First, the optical potential introduces a phase into the (γ, n) matrix element through the distortions of the outgoing neutron wave function. The phase difference $\phi^+ - \phi^-$ due to the real part of the attractive nuclear potential is negative and it increases with l (see the Appendix). Since $\phi^+ - \phi^-$ is already negative (without the optical model correction) because the $E1$ resonance lies below the $E2$ resonance, the correction adds to the phase difference (see Fig. 5). This additional phase difference has the effect of moving the asymmetry curve to higher energy. The magnitude of this shift, due to real part of the potential, increases with l and can be observed in the DSD calculations to states of different angular momentum (Fig. 12). The phase difference due to the imaginary part of the potential is found to be relatively small. The mean shift of the asymmetry curves due to the optical potential (averaged over l) is upward in photon energy. To fit the data would therefore require a lower rather than a higher resonance energy in the DSD calculation than in the semiclassical calculation. This shift is therefore in the wrong direction to explain the discrepancy between the resonance energy assignments in the two treatments. There must therefore be additional differences between these treatments which move the DSD asymmetry curves down in energy.

(ii) The second effect in the DSD calculation which is not present in the semiclassical formulation is the inclusion of a direct component as well as the resonant component for the odd parity excitation. The addition of a nonresonant component makes ϕ^- less negative and increases the magnitude of the phase difference $\phi^+ - \phi^-$. This is in the same direction as the preceding effect but is much smaller.

(iii) The third phase-dependent difference between the DSD and semiclassical treatments is that the numerator of the resonant term is taken to be complex rather than

real in the former in order to represent coupling to other modes. The resulting phase shift of the amplitude comes from the surface region of the nucleus because of the character of the form factor [Eqs. (13) and (15)] and is larger for $E2$ than $E1$ excitation because of the difference in weightings (r^2 vs r) for these excitations. The effect is to reduce the magnitude of $\phi^+ - \phi^-$. This effect results in a downward energy shift of the calculated asymmetry curves and is in the right direction to explain why the E_R value deduced from the DSD calculation lies higher than that from the Breit-Wigner semiclassical treatment. A DSD calculation using a reduced value for the imaginary coupling shows that the use of a complex numerator does indeed move the asymmetry curves down by a few MeV and that this shift is rather independent of the l value.

It is unfortunate that the assignment of the IVQ resonance energy E_R depends as sensitively as it appears to on higher order effects in the excitation of the collective mode. This is particularly so with regard to the effect of the assumed imaginary part of the resonant form factor since there is not yet available a convincing derivation of its form or magnitude.

b. The width of the IVQ resonance. The semiclassical treatment clearly overestimates the width of the IVQ resonance because it tacitly assumes that the energy dependence of the asymmetry curves is independent of l . We have seen that due to the attractive potential for neutrons, the DSD-calculated asymmetry curves for final single hole states of different l are displaced from one another. Our own DSD calculations (Fig. 12) and those of Longo *et al.*³¹ show an appreciable difference in the computed asymmetry curves for different final hole states. Since the measured asymmetry is actually an average over such asymmetry curves [Eq. (3)], it is clear that if these curves happen to be displaced from one another in excitation energy, their sum will give rise to an asymmetry curve with smaller slope than that of any of the individual curves. This would then be taken to correspond to a larger $E2$ isovector width than would match any of the individual curves of Fig. 12.

It would be useful to confirm the strong l dependence of the calculated curves by measuring the asymmetries to individual final states rather than to a superposition of states as we have had to do in this experiment. The sharper rise that was observed in the asymmetry of the earlier $^{208}\text{Pb}(n, \gamma)$ study⁸ (compared with that of the present data) might be accounted for by the fact that a single final state was involved in that experiment.

In any event, one must assume at this point that the IVQ resonance width is closer to that deduced through the DSD calculation than it is to that from the semiclassical model.

c. The strength of the IVQ resonance. Neither model can be trusted for a reliable estimate of the observed strength of the IVQ resonance. There is no way to judge from the excitation functions how much of the cross section is due to the IVQ and how much to other excitations. The asymmetry curves are not much more helpful than the cross-section curves. The observed asymmetry is only weakly dependent on the ratio A^+/A^- and there is,

moreover, considerable uncertainty about the contributions to these amplitudes from the various excitation modes. There is also uncertainty in the relative amounts of direct and collective $E1$ amplitudes.

2. The energy dependence of the (γ, n) cross section

We close this section with a comment on the calculated and observed (γ, n) cross sections as a function of photon energy. It has already been remarked that this cross section in the semiclassical calculation is expected to fall off more slowly with energy than the actual cross section since the (energy-dependent) neutron branching ratio was omitted in that calculation. Figures 11 and 14 show that we have a similar discrepancy between the DSD calculation and experiment, although here the branching ratio is presumably being taken into account.

We have already remarked about the uncertainties in the magnitudes of A^+ and A^- . These uncertainties are even more serious for estimates of the cross sections than they are for estimates of the asymmetries.

V. SUMMARY

The forward-to-backward asymmetry of the (γ, n) reaction to a band of low-lying states has been measured for ^{nat}Pb and ^{nat}Cd in the photon energy range from 20 to 30 MeV. The asymmetries were found to increase from small values (≈ 0.2) to large ones (≈ 0.6 – 0.8) for the two targets. This asymmetry is attributed to an interference between an isovector quadrupole collective resonance and an odd parity background which is due mainly to the tail of the isovector dipole resonance. Direct-semidirect calculations were carried out for Pb and Cd to determine a best set of parameters for the IVQ resonance by fitting to the observed asymmetries and cross sections. Moderately good fits were obtained for assumed resonances at 23.5 ± 1.5 MeV (with width 6 MeV) for Pb, and at 26.5 ± 1.5 MeV (width 7 MeV) for Cd. The strengths of these resonances were however only 40% and 50% of the respective sum rule strengths suggesting that the $E2$ isovector strength is more broadly distributed than the assigned widths would indicate. It should be emphasized that the present evaluations of the resonance width reflect the large dependence of the asymmetry upon the l of the residual state which the DSD calculation predicts. It would be most useful to confirm this prediction by investigating the l dependence experimentally.

The main advantage of the present method for studying the IVQ resonance arises from the fact that in the IVQ resonance region the odd and even parity amplitudes happen, by chance, to be nearly equal. This near equality makes the fore-aft asymmetry insensitive to the precise ratio of the amplitude magnitudes. The asymmetry then depends mainly on the phase difference between the amplitudes and since one of the amplitudes is going through resonance, this phase difference is changing rapidly. One would think that it would therefore be fairly easy to extract the location and the width of the resonance from the asymmetry data. Although this is to a large extent a

reasonable assessment, we have seen that in dealing with reaction amplitudes rather than just with the intensities one can be very sensitive to the phases of these amplitudes. Unfortunately, some of the important phase factors in the present experiment are relatively uncertain. Although they may not be directly related to the giant resonances, they nevertheless limit the certainty with which the resonance parameters can be extracted from the data despite the unambiguous and even dramatic asymmetries that one observes.

This work was supported in part by the U.S. Department of Energy and the National Science Foundation (under Grant No. NSF PHYS 83-11717).

APPENDIX: THE DEPENDENCE OF THE ASYMMETRY ON ANGULAR MOMENTUM

The DSD calculations of Longo and Saporetti,³¹ as well as our own (see Fig. 12), suggest a definite dependence of the asymmetry on the angular momentum of the residual single-hole state. The larger this angular momentum, the smaller the asymmetry. The main source of this dependence appears to be the phase-shift difference between the even- and odd-parity emissions arising from the attraction between the emitted neutron and the residual nucleus.

When the DSD calculation for the (γ, n) reaction is carried out in terms of the inverse reaction (see Sec. IV) the incoming neutron wave is distorted by the attractive potential. The distortion introduces a phase factor $\exp(i\delta_l)$ into each partial wave, where δ_l is the asymptotic phase shift due to the nuclear potential for the l th radial wave. If the residual hole state in the (γ, n) reaction is labeled $l-1$, then the main odd and even parity scattering states for the neutron correspond to angular momenta l and $l+1$, respectively. A phase-shift difference, $\Delta_{l-1} \equiv \delta_{l+1} - \delta_l$, occurs between scattering waves of neighboring l . To the extent that the main contributions to the matrix elements for the two interfering amplitudes come from the nuclear surface region where the neutron wave

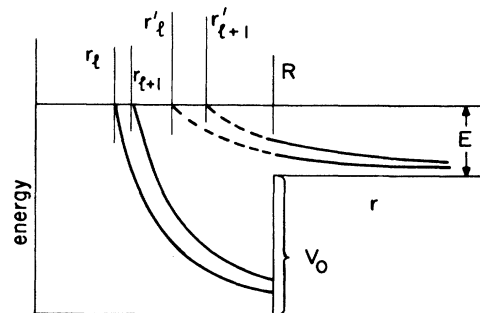


FIG. 15. A diagram to show how one can estimate the difference in phase shifts for neutrons of consecutive l values and the same energy, E , in a square well of radius R and depth V_0 . The curves show the centrifugal potentials up to the classical turning points when the well is present (unprimed r 's) and before it is turned on (primed r 's).

functions have already accumulated almost their full asymptotic phase shift, it is seen that Δ_{l-1} should give a reasonable approximation to the *phase difference* between even and odd amplitudes which arises from the nuclear attraction.

It has been emphasized in this paper that the asymmetries are particularly sensitive to the phase difference between interfering odd and even amplitudes and much less sensitive to the magnitude ratio of these amplitudes. We have therefore carried out a very simple exercise to obtain an approximate estimate for Δ_{l-1} as a function of angular momentum l .

The phase shift for a given partial wave due an attractive potential can be approximated by the difference between the integrals $\int dr/\kappa$ over the classically allowed region when the potential is present and when it is absent. For a neutron of orbital momentum l (we are ignoring the spin), in a three-dimensional square well of radius R this difference is easily shown to be

$$l \left\{ \left[\left[\left(\frac{R}{r_l} \right)^2 - 1 \right]^{1/2} - \arccos \frac{r_l}{R} \right] - l \left[\left[\left(\frac{R}{r'_l} \right)^2 - 1 \right]^{1/2} - \arccos \frac{r'_l}{R} \right] \right\},$$

where r_l and r'_l are the classical distances of closest approach with and without the well (Fig. 15) for the l th partial wave of the neutron.

With reasonable square-well parameters for Pb and with a neutron energy appropriate to this experiment, we find that Δ_{l-1} is negative and that its magnitude becomes rapidly larger as l increases. For impact parameters which correspond to the edge of the Pb nucleus, this phase difference reaches about -30° . The magnitude of the l dependence found in the DSD calculations is qualitatively in accord with that suggested by the square-well exercise.

-
- ¹F. E. Bertrand, Nucl. Phys. **A354**, 129c (1981), and references therein.
- ²R. Pitthan, in *Giant Multipole Resonances*, proceedings, Oak Ridge, TN, 1979, edited by F. E. Bertrand (Harwood Academic, Chur, Switzerland, 1980), p. 161, and references therein.
- ³C. Djalali, N. Marty, M. Morlet, and A. Willis, Nucl. Phys. **A380**, 42 (1982).
- ⁴A. Erell, J. Alster, J. Lichtenstadt, M. A. Moinester, J. D. Bowman, M. D. Cooper, F. Irom, H. S. Matis, E. Piasetzky, U. Sennhauser, and Q. Ingram, Phys. Rev. Lett. **52**, 2134 (1984).
- ⁵D. H. Wright, A. M. Nathan, P. T. Debevec, and L. Morford, Phys. Rev. Lett. **52**, 244 (1984); Phys. Rev. C **32**, 1174 (1985).
- ⁶K. A. Snover, K. Ebisawa, D. R. Brown, and P. Paul, Phys. Rev. Lett. **23**, 317 (1974).
- ⁷G. Longo and F. Saporetti, Nuovo Cimento **61B**, 167 (1969); I. Halpern, in *Proceedings of the International Conference on Photonuclear Reactions and Applications*, Pacific Grove, California, 1973, edited by B. L. Berman (Lawrence Livermore Laboratory, Livermore, CA, 1973), p. 909.
- ⁸D. M. Drake, S. Joly, L. Nilsson, S. A. Wender, K. Aniol, I. Halpern, and D. Storm, Phys. Rev. Lett. **47**, 1581 (1981).
- ⁹I. Bergqvist, R. Zorro, A. Hakansson, A. Lindholm, L. Nilsson, N. Olsson, and A. Likar, Nucl. Phys. **A419**, 509 (1984).
- ¹⁰E. Storm and H. I. Israel, Nucl. Data Tables A **7**, 565 (1970).
- ¹¹F. D. Becchetti and G. W. Greenlees, Phys. Rev. **182**, 1190 (1969).
- ¹²P. T. Debevec, G. L. Moake, and P. A. Quin, Nucl. Instrum. Methods **80**, 467 (1979); N. R. Stanton, Ohio State University report COO-1545-92, 1971.
- ¹³M. Dros, Nucl. Instrum. Methods **105**, 573 (1972).
- ¹⁴J. W. Jury, J. S. Hewitt, and K. G. McNeill, Can. J. Phys. **48**, 1635 (1970).
- ¹⁵B. Bonin, N. Alamanos, B. Berthier, G. Bruge, H. Farragi, D. Legrand, J. C. Lugol, W. Mitting, L. Papineau, A. I. Yavin, D. K. Scott, M. Levine, J. Arvieux, L. Farvacque, and M. Buenerd, Nucl. Phys. **A430**, 349 (1984), and references therein.
- ¹⁶L. J. Morford, Ph.D. thesis, University of Illinois, 1985.
- ¹⁷A. Gavron, Phys. Rev. C **21**, 230 (1980).
- ¹⁸E. K. Warburton and J. Weneser, in *Isospin in Nuclear Physics*, edited by D. H. Wilkinson (North-Holland, Amsterdam, 1969), p. 173.
- ¹⁹A. Veyssiere, H. Beil, R. Bergere, P. Carlso, and A. Lepretre, Nucl. Phys. **A159**, 561 (1970).
- ²⁰R. Pitthan, F. R. Buskirk, E. B. Dally, J. N. Dyer, and X. K. Maruyama, Phys. Rev. Lett. **33**, 849 (1974).
- ²¹C. F. Clement, A. M. Lane, and J. R. Rook, Nucl. Phys. **66**, 273 (1965); **66**, 293 (1965).
- ²²K. A. Snover, in *Neutron Capture Gamma-Ray Spectroscopy*, edited by R. E. Chrien and W. R. Kane (Plenum, New York, 1979), p. 319.
- ²³H. R. Weller and N. R. Roberson, Rev. Mod. Phys. **52**, 699 (1980).
- ²⁴L. Rosen, J. G. Beery, A. S. Goldhaber, and E. M. Auerbach, Ann. Phys. (N.Y.) **34**, 96 (1965).
- ²⁵M. Potokar, A. Likar, M. Budnar, and F. Cvelbar, Nucl. Phys. **A277**, 29 (1977).
- ²⁶K. Ebisawa, Ph.D. thesis, University of Washington, 1978 (unpublished).
- ²⁷S. A. Wender, N. R. Roberson, M. Potokar, H. R. Weller, and D. R. Tilley, Phys. Rev. Lett. **41**, 1217 (1978).
- ²⁸A. Likar and R. Martincic, Nucl. Phys. **A350**, 74 (1980).
- ²⁹C. W. DeJager, H. DeVries, and C. DeVries, At. Data Nucl. Data Tables **14**, 479 (1974).
- ³⁰I. Bergqvist, D. M. Drake, and D. K. McDaniels, Nucl. Phys. **A191**, 641 (1972).
- ³¹G. Longo, F. Saporetti, and R. Guidotti, Nuovo Cimento **46A**, 509 (1978).
- ³²S. Gales, G. M. Crawley, D. Weber, and B. Zwieglinski, Phys. Rev. C **18**, 2475 (1978).
- ³³K. F. Liu and G. E. Brown, Nucl. Phys. **A265**, 385 (1976).
- ³⁴B. Rosner, Phys. Rev. **136**, B664 (1964).
- ³⁵A. Lepretre, H. Beil, R. Bergere, P. Carlos, A. De Miniac, and A. Veyssiere, Nucl. Phys. **A219**, 39 (1974).
- ³⁶C. M. Roza, D. H. Youngblood, J. D. Bronson, Y.-W. Lui, and U. Garg, Phys. Rev. C **21**, 1252 (1980).